Environmental Sciences Europe

RESEARCH

Open Access

Pilot-scale electro-kinetic remediation of lead polluted field sediments: model designation, numerical simulation, and feasibility evaluation

Xinyu Mao[1,2*], Xiaohou Shao[1,2] and Zhanyu Zhang[1,2]

Abstract

Background: The accumulation of lead (Pb) in sediments from anthropogenic activities possesses serious threats to ecosystem and human health. Recycling of sediments for agricultural plantation is politically encouraged while their applications are still limited due to the high cost and poor environmental compatibility of existing remediation techniques. Electro-kinetic remediation (EKR) enhanced with electrode polarity inversion (EPI) strategy was an effective technique for Pb decontamination from low permeable matrix. However, lacking full understanding of the interactions between Pb and sediment constituents restricts the wide application of this technology.

Results: In this study, an innovative approach based on model simulation and feasibility analysis was proposed for guiding the pilot-scale remediation and recycling of Pb-polluted sediments. Initially, a specific two-dimensional (2D) model that consisted of transport-reactive modules was designed, with assumptions of operating parameters and reaction equations. A three-step sequential non-iterative split-operator computation scheme was implemented to simulate the electrochemical variables of EKR. The predicted results indicated that the electrode reversal should be conducted around 48 h to avoid pH polarization and Pb precipitation. In addition, 12 h was suggested to be the preferable EPI duration as the shortest time required (226 h) to remove the target level of sediment Pb. Afterwards, a comparative study was performed between the experimental and simulated data to validate the model accuracy. Good agreements were achieved in spite of minor discrepancies which suggested the designed model could approximately predict the performance of EPI-enhanced EKR. Finally, the feasibility analysis was conducted based on a parametric study. In consideration of energy utilization efficiency, concentration of 220 mg/kg was determined as the lower limit of safety threshold for Pb removal. In this level, the maximum energy consumption (EC), materials, electrolyte post-treatment, and labor expenditure for sediments remediation were 110 \$/m^3, 450 \$/remediation unit, 2 \$/L, and 300 \$/remediation unit, respectively, and the agricultural eco-environment was safe during the recycling process.

Conclusion: We believed that the methodology and results in this study could be employed as an useful tool to support the designation of full-scale EKR and the reutilization of contaminated sediments.

Keywords: Pb-polluted sediments, Pilot-scale decontamination, Electro-kinetic remediation, Electrode polarity inversion, Numerical modeling, Ecology risk evaluation

*Correspondence: mxy880731@163.com
[1] College of Agricultural Engineering, Hohai University, Nanjing 210098, China
Full list of author information is available at the end of the article

Background

For navigational purpose, periodical dredging of estuarine and coastal sediments is often necessary. Generally, sediments are soil particles in the bottom of the aquatic environment. They are natural sinks of organic matter (OM), carbonates, sulfides, iron oxides, as well as toxic metals. Lead (Pb) is the most common toxic metal accumulated in the sediments due to the industrial and agricultural activities [1–4]. As reported, the concentration of Pb in the top layer of the sediments may be as high as 600 mg/kg, which may possess a great risk to human health and ecosystem safety during its dredging and disposal [5]. Currently, recycling of sediments for agricultural plantation is politically encouraged in consideration of cost-saving. However, their applications are still limited due to the shortages of existing remediation techniques such as requirement of a large space, high cost, low sustainability, and poor environmental compatibility [6–8]. Therefore, development of cost-effective and eco-friendly technology for the recovery of metal-polluted sediments becomes an urgent issue.

The electro-kinetic remediation (EKR) is widely accepted as an effective approach for removing toxic metals from a matrix with low permeable, high salinity, and strong buffering capacity. This technique involves introduction of a direct low-intensity electric field to mobilize the target pollutants through transport mechanisms such as electromigration, electroosmosis, and electrophoresis [9]. Induced by electric field, other complex effects like water electrolysis occur at the surface of the electrodes, which respectively generates the H^+ and OH^- ions at the anode and cathode. These ions are transported towards the oppositely charged electrode which causes acidification and alkalization in treated sediments, respectively. Alkalization effect can result in species precipitation and pores blockage, thus impeding the transport of toxic metals. Electrode polarity inversion (EPI) is the most frequently adopted strategy to prevent this negative effect by exchanging the direction of electric field in certain patterns. It is beneficial for neutralizing the OH^- ions around the initial cathode areas and releasing the immobilized toxic metals from the solid particles [10].

Many studies proved that the EPI-enhanced EKR (EPI-EKR) is able to deal with a wide range of toxic metals (e.g., Pb, Cd, Cu, Cr, Zn, and Ni) [11–16]. However, most of these studies focused on the metal-spiked samples at a laboratory scale, the full-scale remediation of field-contaminated sediments was rarely reported. Lacking full understanding of the transport processes and chemical equilibriums of toxic metals is the main limiting factor to widespread usage of this technique in practical applications. As reported, the decontamination efficiency of EPI-EKR is highly dependent on the interactions between contaminants and sediment substances in pore solution [17]. This shows the importance of choosing preferable operating parameters, which can hardly be estimated through the empirical approach due to the strong non-linearity occurring during the remediation processes [18]. For instance, our previous study determined the optimal timing and duration of EPI which were two significant parameters for improving the removal of toxic metals in the porous matrix [19]. These lab-based parameters are case-specific, while directly introducing them to field-scale applications may lead to the inaccuracy of achievable results. Thus, determination of such operating parameters is usually case by case and may be time-consuming.

In order to thoroughly comprehend the complicated mechanisms and efficiently design the appropriate schemes for a full-scale treatment, modeling becomes an essential tool to deal with the technique issues. Many mathematical models were proposed for the simulation of metal extraction with EKR [20–26]. Most of them coupled with the Nernst–Planck or Poisson equation with finite element method to describe both transportations and reactions taking place during the EKR [27]. Despite the considerable efforts were made on model development, poor agreements existed in comparison of predicted and experimental data. On one hand, the geochemical reactions such as precipitation–dissolution, oxidation–reduction, and adsorption–desorption between the species and matrix constituents were not accurately simulated [26]. They are indeed key factors for precise modeling and the limited case studies and data in literatures were the main reasons for the inaccurate simulations [28]. On the other hand, several important intrinsic parameters (e.g., matrix buffering capacity, electrical conductivity, species diffusion coefficients, etc.) could not be straightforwardly hypothesized based on the preliminary data and often were arbitrarily set due to the lack of suitable numerical packages for model parameter assumptions. As a result, model discrepancies derived from the above-mentioned problems affected the performance and optimization of a full-scale EKR.

Although the detailed investigations were carried out towards EPI-EKR, its feasibility to treat field metal-polluted sediments was not assessed yet. One of the major issues to be considered is cost, which is significantly correlated to energy consumption (EC). Unlike soils, sediments with a large presence of OM and carbonates are usually characterized by a high sorption and a buffering capacity. These characteristics may lead to an undesirable energy loss during the remediation. Moreover, energy loss also occurs when electric current passes through the electric wires and electrodes, which are regarded as the additional resistances of EKR system. In many

cases, particular focuses were not given to discriminate between energy losses and energy used effectively for remediation. Thus, cost minimization by improving the conductivity of sediments and selecting the proper materials for electric components was often neglected.

Considering the recycling of sediments for agricultural plantation, evaluation of the relevant ecological risks caused by toxic metals is another important issue for feasibility analysis. At present, Nemerow index, enrichment factor, geoaccumulation index, and potential ecological risk index are common methods for the assessment of soil metal pollution [29–32]. However, some of these methods were not originally developed for such a purpose and the parameters and formulas included may not accurately calculate the contamination index of soil system. In addition, the analysis of metal pollution in agricultural products is not contained in current work, which significantly influences the scientific reliability of evaluation consequences.

To overcome the above-mentioned limitations, a model-based approach was proposed for the full-scale treatment and recycling of Pb-polluted sediments with EPI-EKR. The work included the designation and numerical implementation of a two-dimensional (2D) reactive-transport model with the software of COMSOL Multiphysics® and PHREEQC. The model fully described the transport mechanisms as well as geochemical reactions of Pb in sediments. Particular focus was given to the assumptions of model parameters for better construction of the real contaminated sediment environment. The timing and duration of EPI were optimized based on the simulation results of pH profiles, Pb mobilizations and distributions, and Pb removal efficiencies. The accuracies of the predicted results were then validated through comparing with the experimental data of the pilot-scale EKR tests. Subsequently, a parametric study was performed to analyze the EC of EKR with optimal operating parameters. Minimization of the remediation cost was conducted based on the energy utilization efficiencies and control standards of Pb concentration in sediments and soils. Finally, an innovative method was applied to estimate the ecology risks in agricultural soils and products induced by the recycling of treated sediments. The developed methodology and achieved results in this study may be regarded as a guidance for the cost-effective decontamination and eco-friendly recycling of metal-polluted sediments.

Methods

Sediment sampling and characterization

The sediment samples were collected from the top layer (10–30 cm) of Liqing harbor (32°23′ N, 118°80′ E), which is located close to the industrial estate of Luhe district in Nanjing city, Jiangsu Province, China (Fig. 1). The dredged sediments were kept in cool conditions (− 20 °C) and stored in airtight plastic barrels during transport. Pretreatment of homogenization including dewatering, air-drying (72 h), and sieving (2-mm sieve) were conducted before the experiments. Sediment physico-chemical properties and relevant analytical methods were summarized in Table 1. All the analytical procedures were applied in triplicate. Major elements and heavy metal(loid)s were extracted after acid digestion and the contents in solution were determined with inductively coupled plasma mass spectrometry (ICP-MS). As a target pollutant, the speciation of Pb in investigated sediments was analyzed through BCR sequential extraction method and the total Pb was about 346 mg/kg.

Layout of the treatment system

The diagram of the pilot-scale EKR plant was schematically presented Fig. 2a. It consisted of rectangular basin ($L \times W \times H = 12\ m \times 10\ m \times 4\ m$) to contain a volume of 360 m^3 polluted sediments. The basin was divided into eight equivalent remediation units (Fig. 2b) with twelve electrode wells inserted for the installation of electrodes. The arrays of the electrode wells were equidistantly distributed and the unit distance in the vertical and horizontal direction was about 2.7 m and 4.7 m, respectively. The electrode wells were connected to the electrolyte management system by PVC pipes for electrolyte circulation. Graphite electrode rods ($L \times \Phi = 360\ cm \times 20\ cm$) were applied as both anode and cathode and connected to a DC power supplier at a constant voltage potential of 0.5 V/cm. The dredged sediments in the basin were treated in a unit-by-unit order as shown in Fig. 2b. A sensor-based monitoring system was used to record the variations of sediment pH and passing electric currents. The replaced electrolyte (0.1 M KCl) and generated noxious gas (Cl_2) were, respectively, transferred to the electrolyte purification and gas scrubbing systems for post-treatment.

Model designation

Initialization

Some operating parameters were initially assumed for model implementation. The major migrating species considered in the polluted sediments were H^+, OH^-, K^+, Cl^-, Pb^{2+}, $PbCl^+$, $PbCl_3^-$, $PbCl_4^{2-}$, and $PbCl_2$. These species hold significant contents at working conditions and around 13% of the total Pb was considered as Pb^{2+} based on the speciation analysis. The same diffusion coefficient was assigned to Pb^{2+} and its aqueous complexes according to the literature [33]. Before transport, reactions of precipitation and dissolution were hypothesized to occur between the soluble and solid phases of sediment Pb. The solid phases taken into

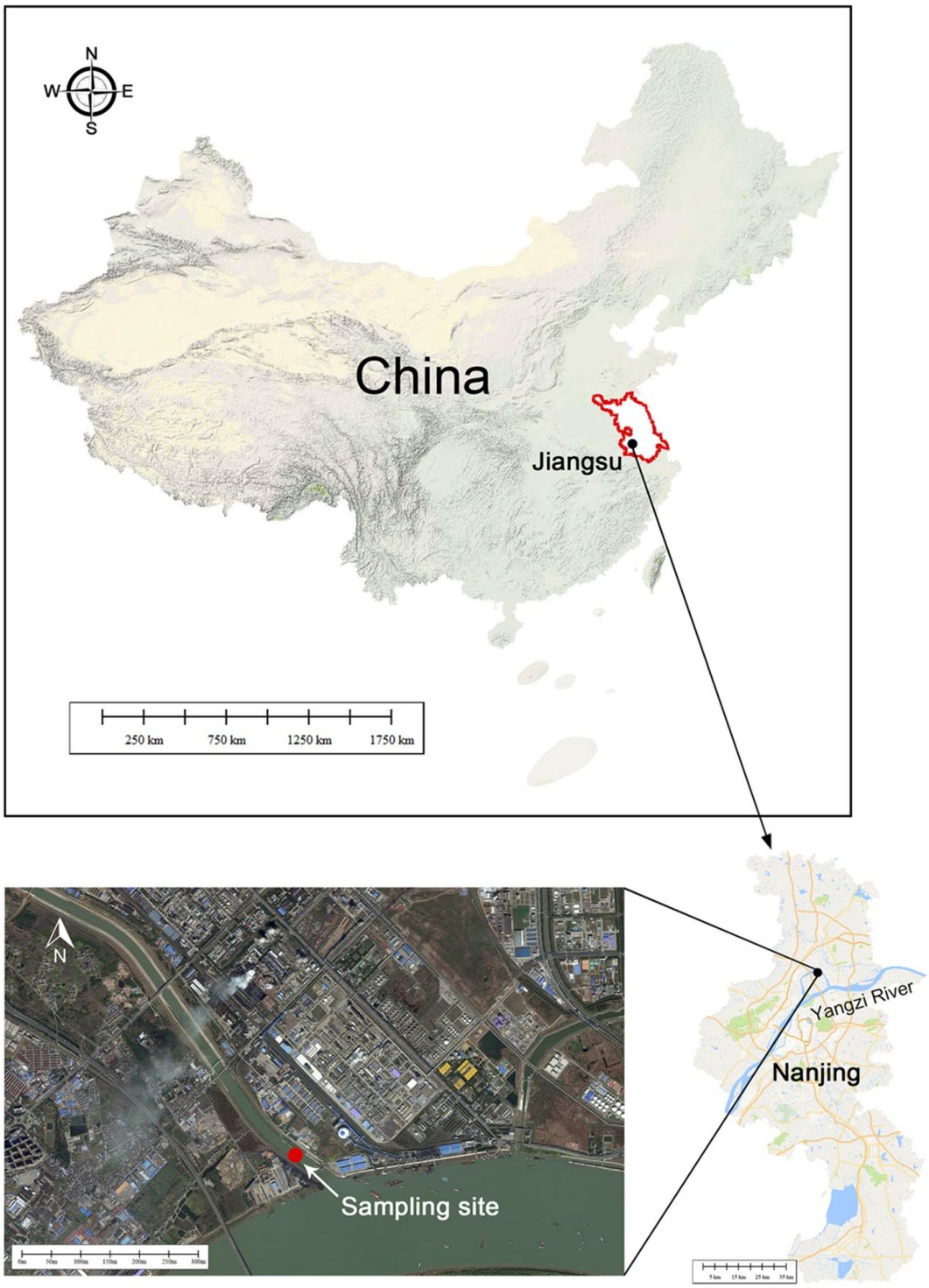

Fig. 1 Sampling site map of Liqing harbor in Luhe district of Nanjing city, Jiangsu Province, China

account in the model included $Pb_3(OH)_2(CO_3)_2$, $Pb(OH)_2$, and $PbCO_3$. The equilibrium constants for the precipitation and dissolution of Pb were referred to the thermodynamic database of PHREEQC [34].

In addition, some other conditions were also assumed in order to simplify the model. The electric potential that distributed along the vertical direction was neglected, reflecting in the presentation of the actual 3D geometric

Table 1 Physico-chemical properties, major elements, and heavy metal(loid)s of the experimental sediments

Properties	Methods	Unit	Value
Grain size distribution			
d > 2 mm	ASTM D 421	%	0
0.063 mm < d ≤ 2 mm			54.2 ± 2.7
d ≤ 0.063 mm			45.8 ± 3.8
Porosity	ASTM D 854	%	46.2 ± 4.5
pH	US-EPA 9045d		6.8 ± 0.44
Buffering capacity			
to pH − 2.0 ± 0.2	ASTM D4972	mol H^+/kg	21.24
to pH − 13.0 ± 0.2		mol OH^-/kg	0.96
Water content	ASTM D 2980	%	31.4 ± 2.2
Electrical resistivity	ASTM D 5682	Ω m	0.75 ± 0.13
Electrical conductivity	ASTM D5298	mS/cm	13.4 ± 1.6
CEC	US-EPA 9081	cmol/kg	124.6 ± 8.3
Sulfur	US-EPA 9031	%	0.32 ± 0.02
Nitrogen	US-EPA 351.2	%	0.56 ± 0.04
OM	ASTM D 2974	%	12.3 ± 1.2
DOM	ASTM D7573	mg/kg	16.5 ± 1.7
Carbonate	ASTM D 4373	%	26.4 ± 4.3
Total carbon	ASTM D 5997	%	6.2 ± 0.93
Metals/salts			
Ca	US-EPA 6020	mg/kg	6840 ± 560
Fe			8800 ± 420
Al			7260 ± 340
Mg			5050 ± 410
Mn			105.6 ± 8.2
K			2520 ± 340
Na			6380 ± 460
P			1540 ± 120
Heavy metal(loid)s			
Cu	US-EPA 6020	mg/kg	83.7 ± 5.3
Zn			43.8 ± 3.2
Cd			0.8 ± 0.1
As			15.4 ± 1.8
Ni			16.2 ± 2.1
Cr			26.7 ± 4.6
Pb			
EXT[a]			44.8 ± 4.2
OXID[b]			98.8 ± 8.7
RED[c]			176 ± 12.4
RES[d]			25.7 ± 4.8

[a] Acid extractable fraction

[b] Oxidizable fraction

[c] Reducible fraction

[d] Residual fraction

remediation setup with a 2D model. The advective flow and electrophoresis that contributed to Pb transport were not considered due to the low hydraulic permeability of the experimental sediments. The pore geometry of the sediments was assumed to be isotropic with fixed porosity and tortuosity during the remediation. Moreover, the sediment water content was regarded to be constant with a saturation degree of 100% due to continuous complement of the electrolyte.

Governing equations

Two coupled modules that described the transport processes and chemical equilibriums made up the model. In transport module, the ionic species were assumed to migrate through electromigration and electroosmosis under electric force. Their flux densities J_i (mol/m^{2}s) passing through the cross-sectional area of the sediments were described as

$$J_i = -D_i^* \nabla c_i - U_i^* c_i \nabla \phi - k_{eo} c_i \nabla \phi, \quad (1)$$

where i represents the species, D_i^*(m^2/s) and C_i (mol/m^3) are, respectively, the effective diffusion coefficient and content of ith specie, ϕ(V) denotes the voltage, U_i^* (m^2/V s) is the effective ionic mobility coefficient, and keo(m^2/V s) is the electroosmosis permeability coefficient.

The transport of ionic species was further expressed by Nernst–Planck equation in consideration of mass conservation:

$$n\frac{\partial ci}{\partial t} = -\nabla \times \left[-D_i^* \nabla ci - \left(U_i^* + keo\right) ci \nabla \phi\right] + nGi, \quad (2)$$

where n is the porosity of sediments, t (s) is the elapsed time, and G_i (mol/m^{3}s) is the generated volume of ith specie via chemical reactions. Since the pathway for ion migration in porous medium is tortuous, the effects of sediment porosity (n) and tortuosity (τ) were taken into account to define the D_i^* and U_i^* in Eq. (2) as

$$D_i^* = n\tau D_i, \quad U_i^* = n\tau U_i. \quad (3)$$

The porosity was predetermined in Table 1 and the tortuosity was assumed to span in a range of 0.01–0.84 depending on the physico-chemical properties of the sediments [35]. The relationship between D_i^* and U_i^* could be defined by Einstein–Nernst relation as a single property:

$$U_i^* = \frac{D_i^* Z_i F}{RT}, \quad (4)$$

where R (8.314 J/K mol) and F (96,485 C/mol) are the ideal gas constant and Faraday's constant, respectively, Z_i is the ionic charge of ith specie, and T (K) is the absolute temperature.

According to Helmholtz and Smoluchowski's theory, the keo in Eqs. (1) and (2) is an integrated function of porosity n, liquid dielectric constant ε (F/m), zeta

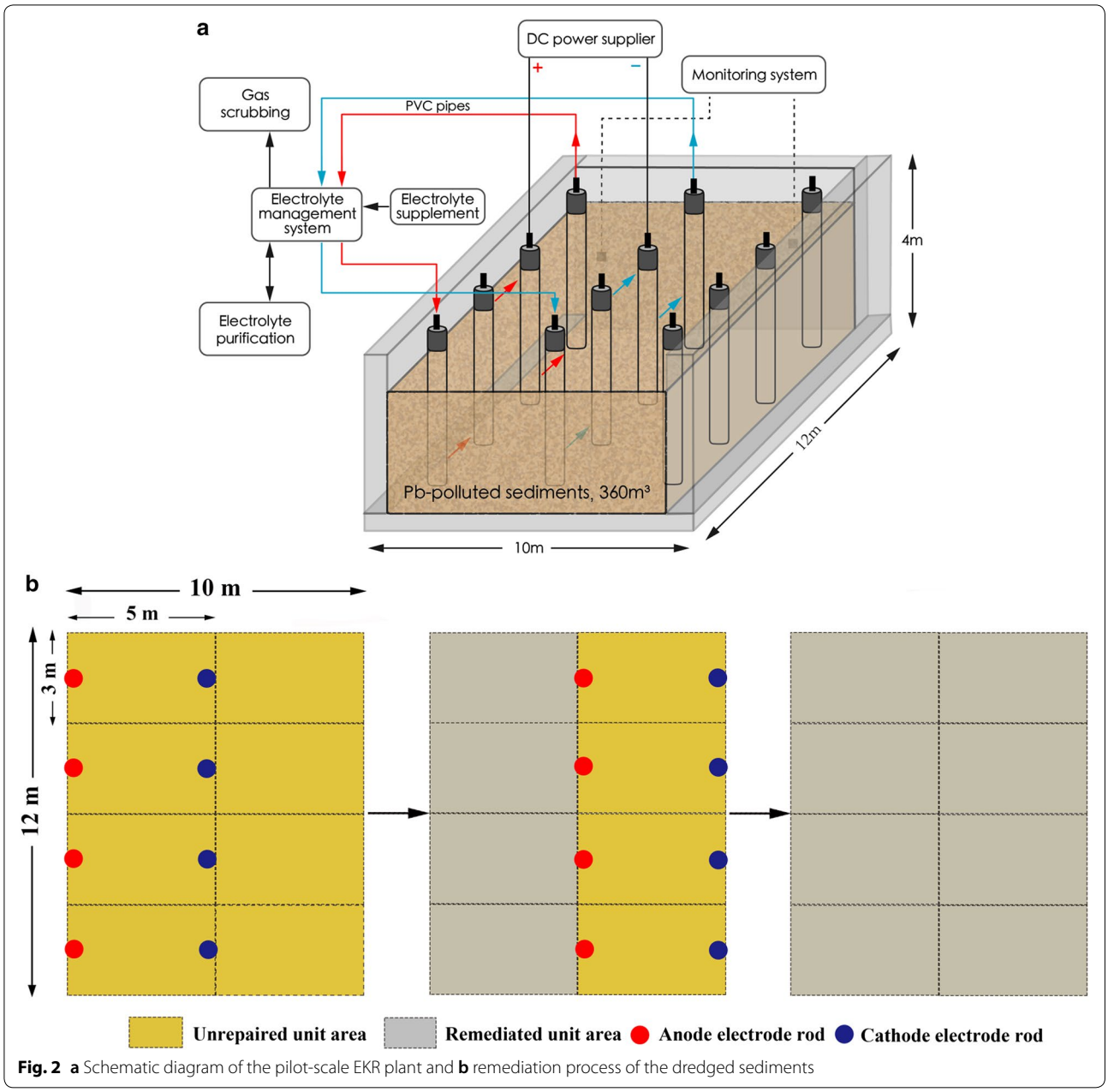

Fig. 2 **a** Schematic diagram of the pilot-scale EKR plant and **b** remediation process of the dredged sediments

potential ζ (V), and fluid viscosity η (N s/m^2) of the porous matrix [36]:

$$k_{eo} = n\frac{\varepsilon\zeta}{\eta}. \tag{5}$$

In this equation, the values of porosity and liquid dielectric constant were listed in Table 1, and the viscosity of the electrolyte (0.1 M KCl) was about 1.12-fold compared to that of water referred to Qiu's report [37]. As a result, the zeta potential becomes the determining factor and can be calculated through the expression of volume-averaged EOF Q_{eo}(m^3/s):

$$Q_{eo} = nA\frac{D\zeta}{\eta}E_z, \tag{6}$$

where A (cm^2) and E_z (V/cm) are, respectively, the cross-sectional area and the electric potential intensity.

In chemical module, the reactions which possess great contributions to sediment decontamination were described via a set of non-linear algebraic equations.

Water electrolysis is one of the main reactions which has electrochemical oxidation and reduction at the surface of electrodes:

$$2H_2O \rightarrow O_2 \uparrow +4H^+ + 4e^- \ (Anode) \tag{7}$$

$$2H_2O + 2e^- \rightarrow H_2 \uparrow +2OH^- \ (\text{Cathode}). \tag{8}$$

The presence of Cl^- ions due to the application of KCl electrolyte resulted in the generation of Cl_2 gas under the same redox potential of water oxidation. However, this effect was neglected in the model since the concentration of added Cl^- was low, which might not be competitive with water oxidation.

The surface complexation is another main reaction that describes the acid buffering capacity of the experimental matrix. It is related to the ion exchange between the generated H^+ and adsorbed metals on the active sites of the solid particles:

$$\equiv SOH + H^+ \rightleftarrows \equiv SOH_2^+; \ \equiv SOH \rightleftarrows \equiv SO^- + H^+, \tag{9}$$

where $\equiv SOH$ represents the active sites of the solid particles and S represents the adsorbed metals. Due to the double-layer structure, the above protonation and deprotonation reactions are mainly dependent on sediment pH without considering electrostatic attraction or repulsion. The reactions were further simulated by a non-electrostatic model to calculate the relevant equilibrium constants:

$$K_1 = \frac{[\equiv SOH_2^+]}{[\equiv SOH][H^+]}; \quad K_2 = \frac{[\equiv SO^-][H^+]}{[\equiv SOH]}. \tag{10}$$

The adsorption and desorption of Pb onto sediment particle surfaces were also modeled by using an adsorption isotherm:

$$S_{Pb}^a = K_d c_{Pb}, \tag{11}$$

where S_{Pb}^a (mol/mg) denotes the concentration of Pb adsorbed on sediment particles, K_d (m^3/kg) denotes the linear distribution coefficient of liquid and solid phases, and c_{Pb} (mol/m^3) denotes the content of Pb in pore liquid.

Numerical implementation, simulation, and calibration

A three-step sequential non-iterative split-operator scheme was implemented to compute the aforementioned transport and chemical processes (Fig. 3). In the first step, some assumptions were made for model initialization. Then, the transport behaviors of dissolved chemical species under a constant voltage were simulated by using the finite element method with COMSOL Multiphysics®. In this step, the chemical phenomena that act as driving factors of the EKR were calculated by PhreeqcRM. Subsequently, the above two steps were integrated with the coupling time arbitrarily set to 5×10^4 s [35]. During the calculation loop, the approach of operator splitting was applied to compute the reactive-transport equilibriums, which minimized the

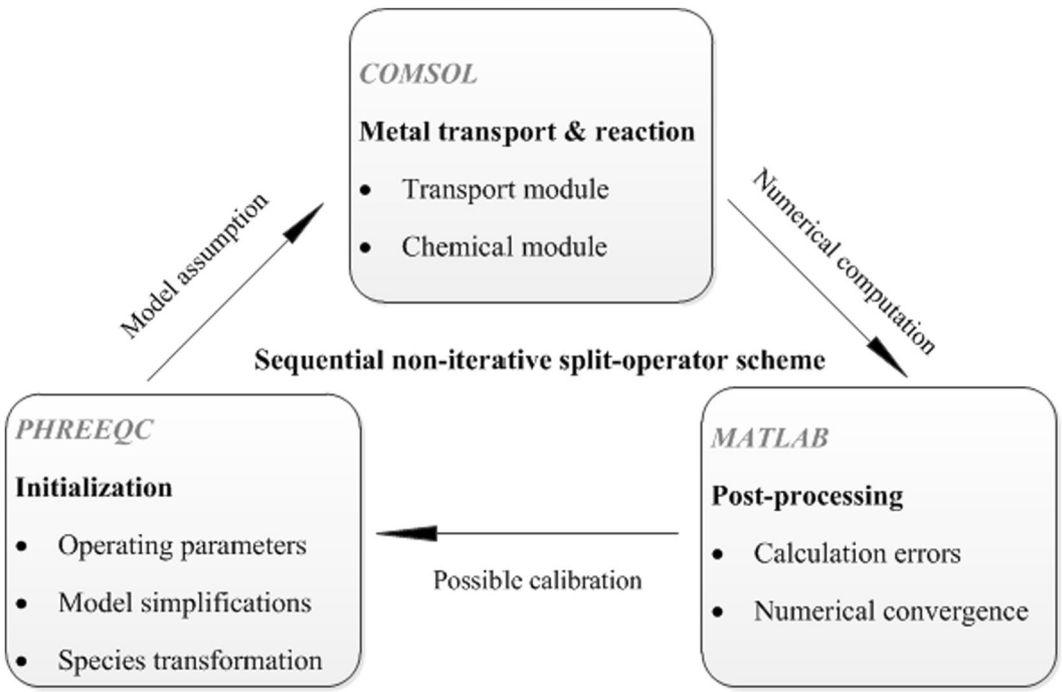

Fig. 3 The three-step sequential non-iterative split-operator implementation scheme of the 2D transport-reactive model

calculation errors and ensured an acceptable computation time. In the last step, numerical convergence was achieved and used for data analysis in post-processing. Possible calibrations could be made according to error adjustments by COMSOL in combination with model validations by comparing the predicted data with the full-scale experimental results.

Energy consumption and cost analysis

The EC for Pb electromigration, voltage drops, and management of EKR system was independently calculated. A specific concept of energy utilization efficiency (β) was defined to describe the relationship between EC and metal removal:

$$\beta = \frac{\eta}{W_i}, \tag{12}$$

where η (mg) is the removal mass of sediment Pb and W_i (kWh) is the relevant EC.

The cost of EC for EKR to remove the target level of sediment Pb was estimated. The minimization of such a cost was conducted based on the energy utilization efficiencies and the safety control standards for sediment Pb.

Ecology risk evaluation

Field plantation experiments were conducted to evaluate the ecology risks induced by the recycling of treated sediments. An innovative approach which comprehensively estimated the qualities of both soils and vegetables was applied. The evaluation method considered the factors of metal valance, environmental standard for soils, background values of soil metals, soil loading capacity of pollution, and food safety control standard for the contaminant, which ensured the scientific reliability of the evaluation results. Vegetables of *Brassica juncea*, *Brassica pekinensis*, and *Spinacia oleracea L.* were chosen for plantation due to their good accumulating ability on soil Pb. They could efficiently accumulate the Pb in roots and transport them to shoots with satisfying translocation factors [38]. In addition, as hyperaccumulator, the accumulation of Pb in *Brassica juncea* should be larger compared to those in *Brassica pekinensis* and *Spinacia oleracea L.* The Pb concentration in soils and vegetables was measured with ICP-MS after harvest. All the experiments were conducted in four replicates and the ecological risks were further classified according to the criterions of agro-ecosystem quality assessment.

Results and discussion

Numerical simulation results

Estimation of EPI timing

The EPI strategy possessed considerable buffering effects on soil pH polarization during the EKR process. It is desirable to alleviate the focusing phenomena such as precipitation of major elements, immobilization of aqueous Pb, and blockage of sediment pores induced by alkalization around the cathode areas. The timing to reverse electrode polarity is important since it directly determines the frequency of EPI and the performance of EKR. For that reason, the appropriate EPI timing was initially evaluated, based on the time-dependent 2D simulations of acidic front and Pb migration with conventional EKR under pilot-scale conditions (EXP 1).

From the obtained results (Fig. 4), the advances of both acid and basic fronts towards the opposite direction were much faster along the main anode–cathode axis, while became slighter in the same longitudinal positions from the median to the border. This phenomenon could be explained by the electric field distribution that the voltage gradient in the middle axis was higher than at the borders of the remediation unit. As a result, the residual Pb content followed the same trend that larger transport of Pb was observed along the central anode–cathode line. The data also showed that intensive pH polarization occurred at 48 h and the pH value close to the anode and the cathode had already polarized to 2.7 and 10.7, respectively. Moreover, a pH jumping point (pH varied from 6 to 9) appeared at that time near the cathode region due to the faster movement of H^+ [39]. This sharp transition of pH led to the precipitation of Pb and an approximately 9.3–19.9% elevation of Pb concentration was showed around the pH jumping section.

The above results demonstrated the fact that the distribution of Pb highly depended on sediment pH. Without pH management, Pb would accumulate in a narrow zone, where stable anionic Pb complexes and precipitations were formed. This zone corresponded to dead areas where Pb^{2+} could hardly pass through, especially in the upper and lower corners. Therefore, reversing electrode polarity at the time that intensive pH polarization appeared was required to promote Pb removal in these areas. In our study, sediment pH polarized significantly after 48 h EKR, which suggested 48 h might be the preferable timing of EPI. It should be noted that this hypnosis was model specific and may not be generalized. Nevertheless, it could be regarded as valid in cases where similar model designations were assumed.

Evaluation of EPI duration

The operating duration of EPI is another important parameter that needs to be confirmed as it significantly influences the decontamination efficiency and energy consumption of the EKR system. Theoretically, it should be determined on account of two basic principles that (1) the sediment pH depolarized to a lightly acidic range which was favorable for the mobilization of Pb and (2)

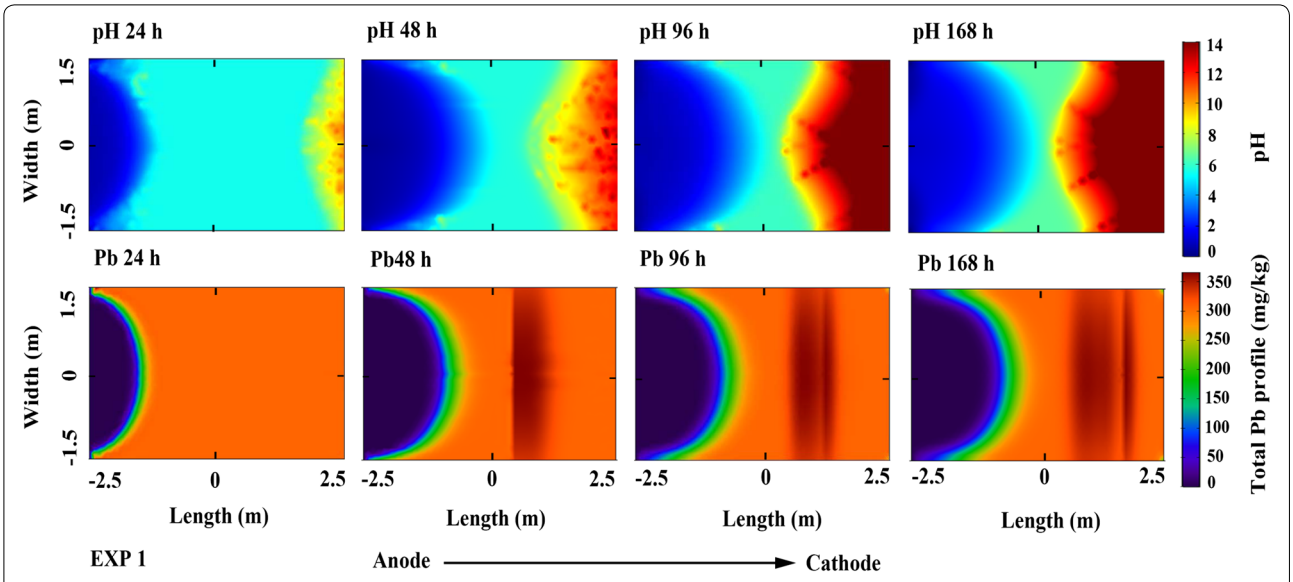

Fig. 4 Time-dependent 2D model results of sediment pH and Pb distributions under conventional EKR (0.5 V/cm)

the immobilized Pb released to the porous matrix without reflux of the aqueous Pb towards the initial anode regions. In this way, three EPI durations of 6 h (EXP 2), 12 h (EXP 3), and 24 h (EXP 4) were assumed for model-based EKR tests, respectively.

As mentioned, the depolarization effect induced by EPI was the main concern. Thus, indicators of sediment pH and Pb distributions in the end of the first three polarity reversions were chosen to describe this effect. From the model results, the sediment pHs were clearly depolarized to different extents as a function of EPI durations (Fig. 5). Regarding to EXP 2, sediment alkalization still existed in 54-h profile and similar patterns were obtained in the following simulations (108 h and 162 h). In terms of EXP 3 and EXP 4, the basification phenomenon close to the initial cathode areas was approximately eliminated and most sediment areas were kept acidic after polarity inversion. Therefore, EPI duration between 12 h and 24 h seemed to be proper since desirable environment for Pb electromigration was established even through slight basification was shown around the initial anode regions of EXP 4.

Referring to the predicted results of Pb distributions (Fig. 6), the dead zone areas in EXP 2 were diminished after polarity reversion. Moreover, the peak concentration of Pb moved towards the initial cathode regions with elapsed time. The accumulation of Pb was totally eliminated in EXP 3 that we suggested all the adsorbed Pb were released to sediment pore solution. This result may be related to the pH distribution. Firstly, entire sediment environment was in acidic range resulting in more Pb^{2+} remobilized from its stable anionic complexes and precipitations via ion exchange [40]. Secondly, due to the acidification effect, more OM in sediments was transformed to dissolved organic matter (DOM) which accelerated the release of immobilized Pb [41]. According to our pre-measurement, a large part of Pb in sediments was OM-bounded (oxidizable fraction) since the large amount of OM. Nevertheless, as the increase of DOM, more soluble organic complexing and exchangeable Pb (acid extractable fraction) could be formed and transported through electromigration and electroosmosis [42]. No obvious backflows of Pb were observed in EXP 2 and EXP 3 during the EPI intervals, while appeared in EXP 4 with a probably 15–25% of Pb around the initial cathode areas transported towards the initial anode areas. Thus, based on the aforementioned model results, 12 h should be the most preferable duration for EPI during the EKR process. This conclusion was further verified through the simulated results of Pb removals in different EKR tests. Figure 7 illustrated the time required to wipe off the sediment Pb to a predetermined target level (90%) and it was ranked as EXP 4 = 586 h > EXP 2 = 367 h > EXP 3 = 226 h.

Model validation

In order to validate the assumption that the designed 2D model could approximately predict the real transport-reactive process in practical remediation, comparisons between the predicted and full-scale experimental results were carried out in both conventional and EPI-EKR tests. For that purpose, the electrolyte was collected every 6 h to measure the Pb extraction mass and removal rate. Furthermore, the sediment samples were collected along

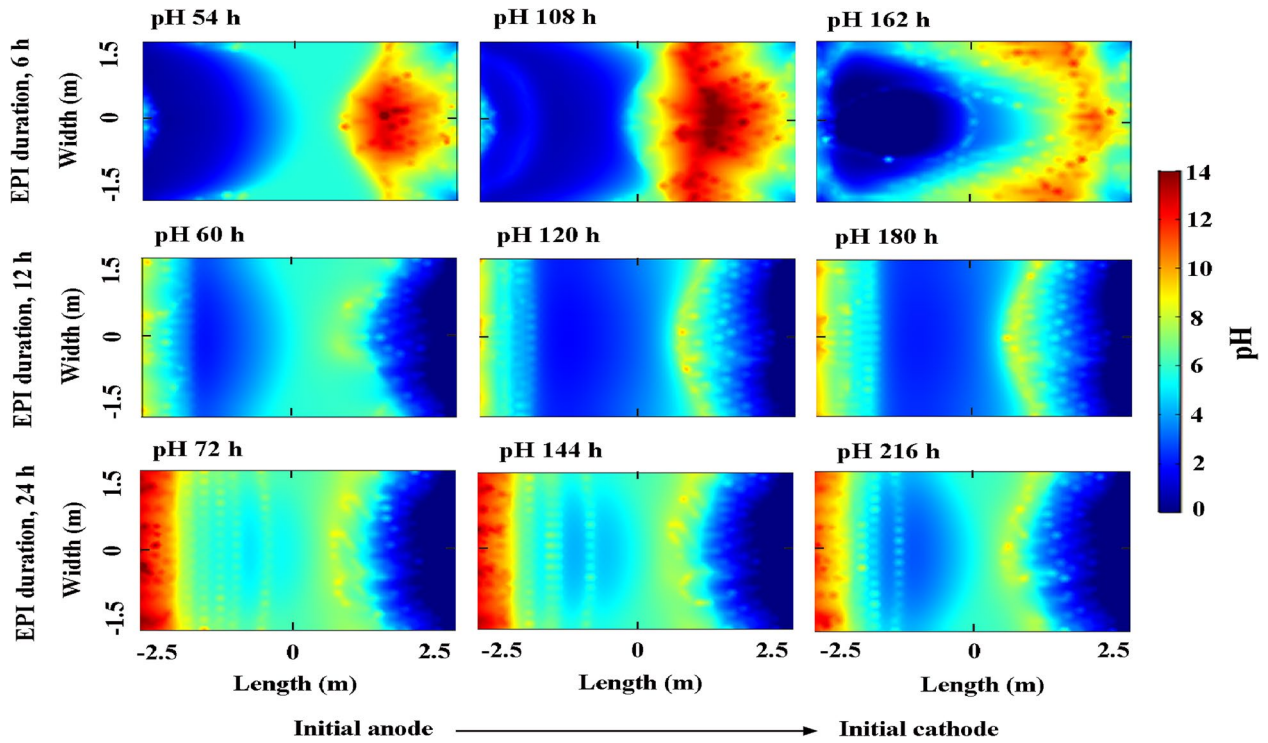

Fig. 5 Simulated sediment pH distributions under EKR (0.5 V/cm) with EPI duration of 6 h, 12 h, and 24 h

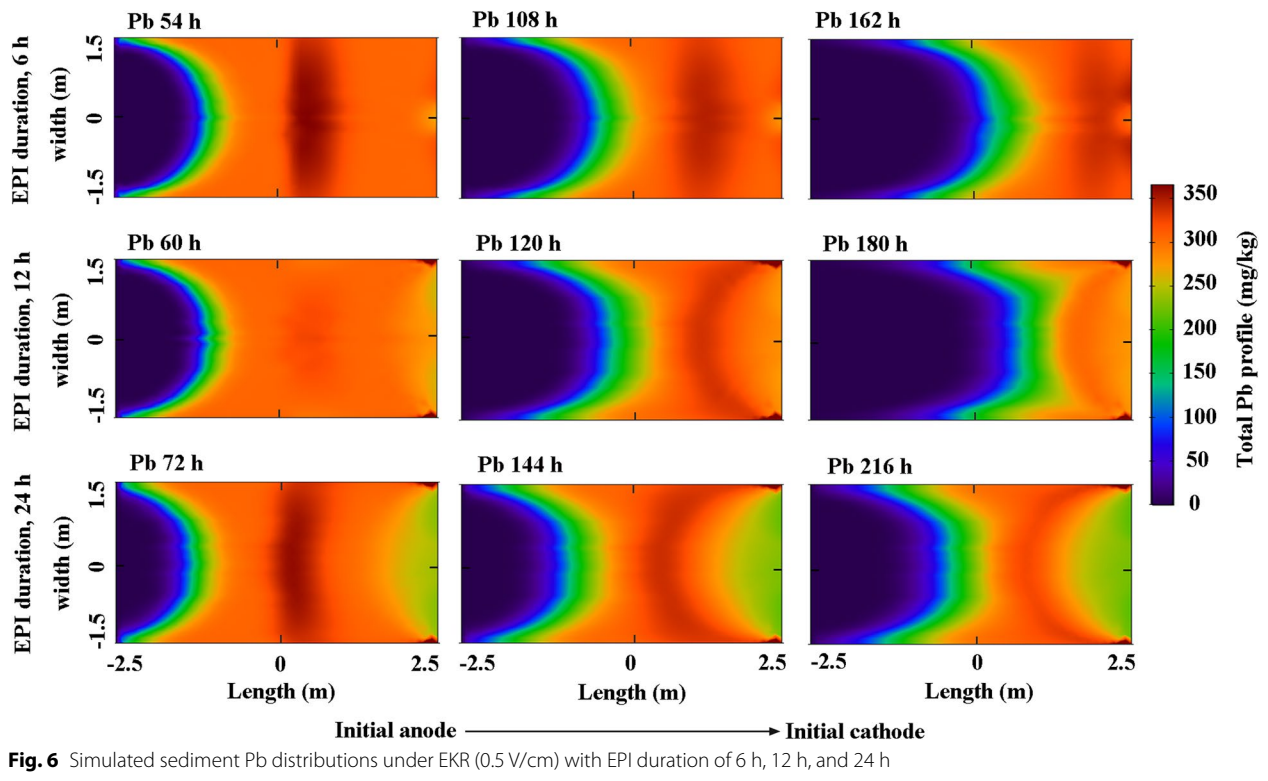

Fig. 6 Simulated sediment Pb distributions under EKR (0.5 V/cm) with EPI duration of 6 h, 12 h, and 24 h

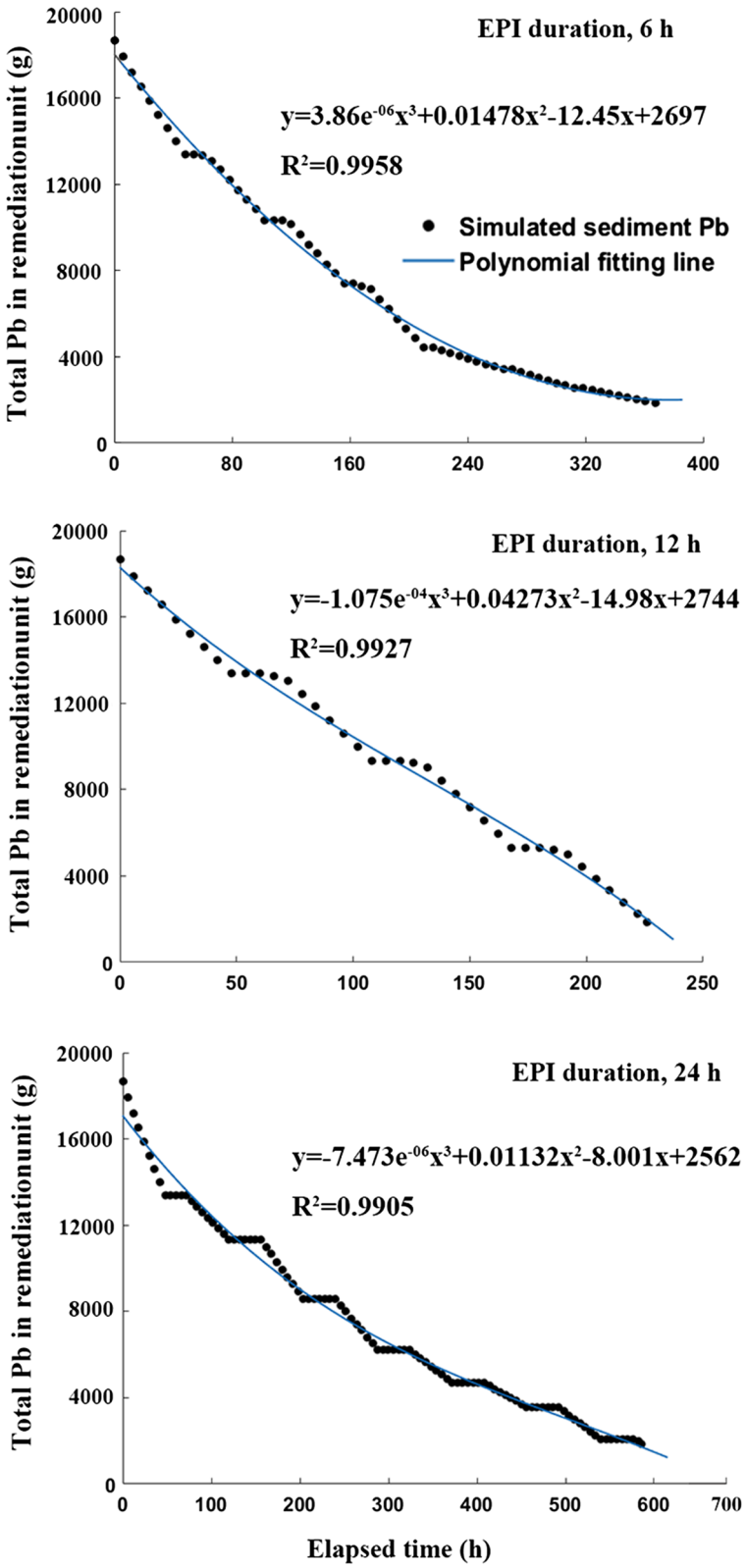

Fig. 7 Simulated Pb removal to a target level of 90% under EKR (0.5 V/cm) with EPI duration of 6 h, 12 h, and 24 h

the main anode–cathode axis in 48 h, 108 h, 168 h, and 228 h, respectively, to measure the pHs and Pb distributions. All the measurements were conducted in triplicate to ensure the good reproducibility and reliable verification from the acquired data.

The validation of simulated Pb extraction mass and removal rate were conducted in EXP 1. From the comparisons (Fig. 8), a good agreement was shown between the modeled and measured data in spite of minor discrepancies. In general, the measured data were slightly lower in the early stage while the differences were magnified after the moment of extraction plateau (around 48 h). This phenomenon might be caused by the simplification of electric field distribution introduced in the model. In fact, the actual electric strength that contributed to Pb electromigration was lower than the assumption due to its effect on the outside of the remediation unit was neglected. Moreover, the voltage drops across the electric wires, electrodes, and sediment matrix were also not considered. Consequently, the experimental Pb extraction mass and removal rate were 5–10% lower than the predicted results and the errors of actual electric field should lay in this range.

The validation of sediment pHs and Pb profiles were carried out in EKR test with optimal EPI duration of 12 h (EPX 3). Figure 9a presented the pH profiles prediction and verification. It showed good accuracy even though some minor standard deviations were appeared in the early data (48 h and 108 h). These slight disagreements, especially around the anode regions, might result from the integrated effects of transport-reactive reactions and ionic strength variations. As reported, matrix with high buffering capacity would experience a slow kinetic-controlled pH buffering process during the EKR [43]. This process would particularly influence the short-term pH distribution. As a result, the mobilization of real acid front in the early stage allocated behind of the results predicted by the model. It should be mentioned that, with continuous depletion of ions in matrix, the ionic strength should be kept decreasing which was assumed as a constant in the model. This effect could slower the movement of acid/basic front in long-term EKR. Nevertheless, excellent agreements were achieved on pH profiles after 108 h which enabled to conclude that the impact of electro-reactions on H^+/OH^- distributions was significantly larger than that of ionic strength variations. The sediment Pb profiles with elapsed time were also predicted with a good accuracy (Fig. 9b) except little overestimation of Pb migration around the initial anode regions. These discrepancies could be due to the stable Pb bonding fractions in the sediment. Considering the premeasured speciation of Pb (Table 1), the residual Pb which accounted for 7.4% of the total Pb was of relevant significance. This fraction is less mobile and holds high resilience to acid front. Accordingly, the Pb content in sediments could not be decreased to zero.

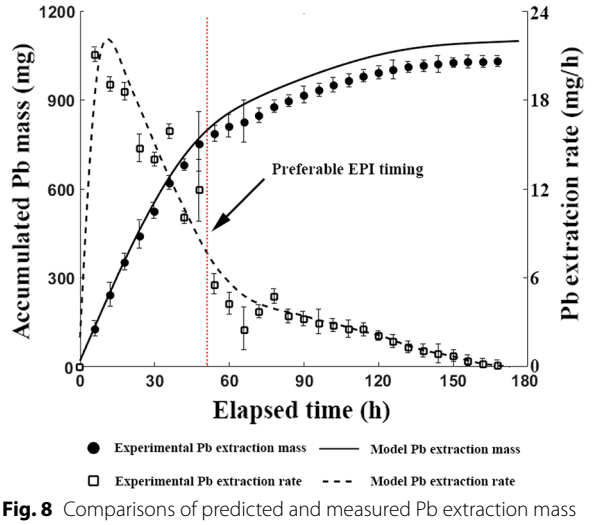

Fig. 8 Comparisons of predicted and measured Pb extraction mass and removal rate under conventional EKR (0.5 V/cm). The preferable EPI timing referred to the moment that stable anionic Pb complexes and precipitations were largely formed due to the intensive alkalization effect

Feasibility analysis

Energy consumption and cost assessment

In order to demonstrate the feasibility of the optimal EPI-EKR for sediment Pb decontamination, a parametric study of EC and relevant cost per remediation unit was performed. The EC taken into account were EC for Pb electromigration, voltage drops across the electric wires, graphite electrodes, and sediment matrix, and management of EKR system. They were quantified as a function of applied voltage (V) and current intensity (I) with elapsed time (t). Particularly, the power dissipated outside the remediation zone for Pb electromigration was neglect. In fact, this energy loss was estimated to be less than 5 W/m^3 according to the model computation. The voltage drops (ΔV) were simply described as the additional resistances from power source to anode (ΔV_{An}) and from anode to cathode (ΔV_{Cat}), respectively:

$$\Delta V = \Delta V_{An} + \Delta V_{Cat} = I\left[\sum_{i=1}^{N} \frac{\rho_i L_i}{S_i}\right], \tag{13}$$

where the electric current (I) was presimulated as a linear transfer function of $I = -0.015\ t + 13.9$, i is the component that electric current passing through, N is component's number, and ρ_i (Ω m), L_i (m), and S_i (m^2) is its resistivity, length, and cross-sectional area,

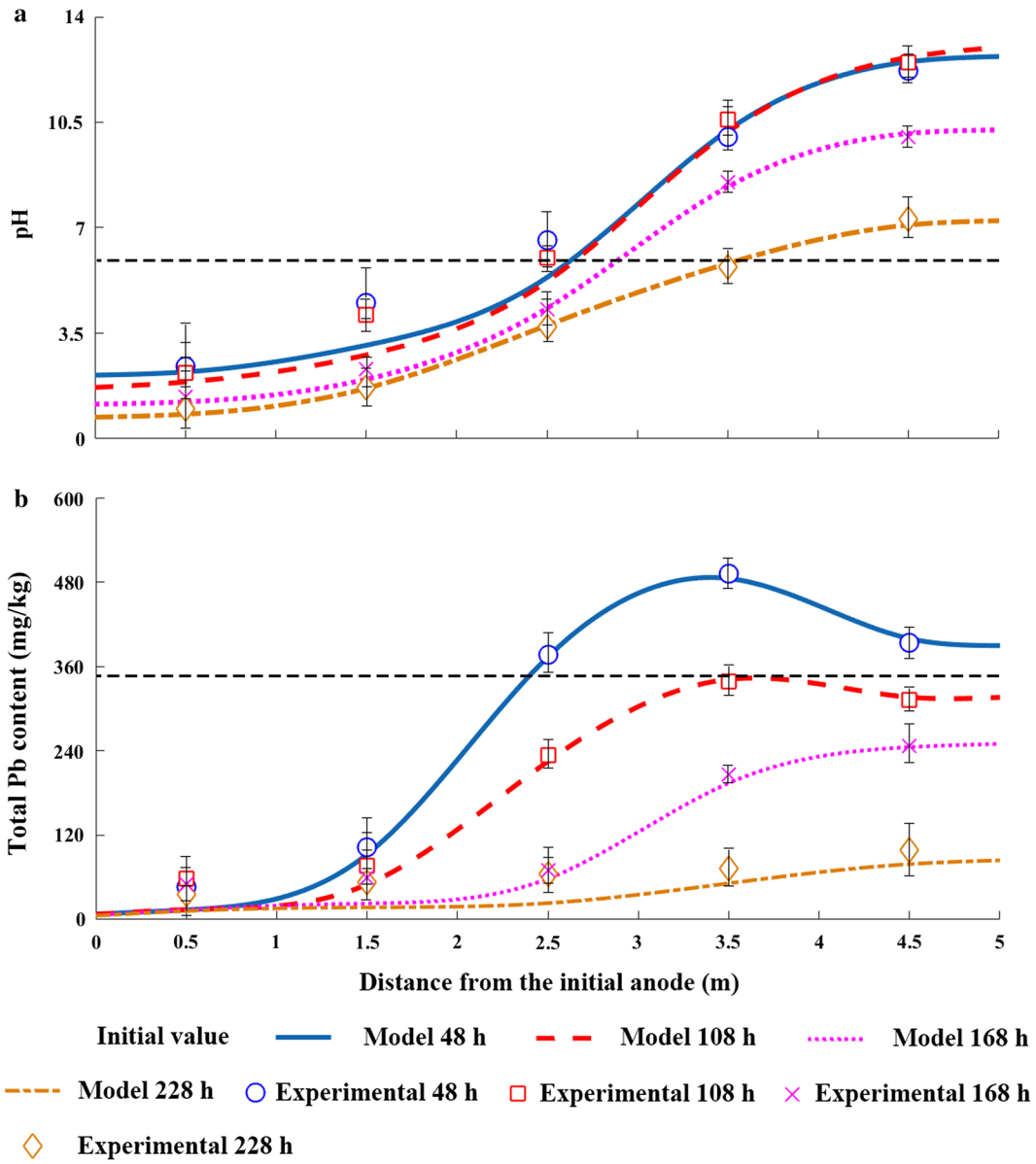

Fig. 9 Validation of simulation: pilot experimental data plotted versus simulated pH (**a**) and Pb distributions (**b**) alone the median anode–cathode axis under EKR (0.5 V/cm) with optimal EPI duration of 12 h

respectively. The management of EKR system mainly included sediment pH monitoring, electrolyte supplement, and electrolyte circulation. Here, we suggested a total power (P) of 10 W/m^3 to run such managing instruments. A summary of the assumed parameters and relative unit values was shown in Table 2. Subsequently, the assumptions allowed us to calculate the time-dependent EC with the following relationship:

$$EC = (V - \Delta V)It + \Delta VIt + Pt. \quad (14)$$

From this relationship, we were able to discriminate between energy losses and energy used effectively for remediation. Figure 10a showed the results of the referred EC. All the EC had an increasing trend with time and the total energy to remove 90% of the sediment Pb was 413 kWh. The energy expenditure caused by voltage drops and EKR system management only accounted for around 7–9% of the total EC, which might imply an approving energy utilization efficiency. For better understanding of the energy utilization

Table 2 Parameters and unit values of assumed components for energy consumption and cost assessment

Parameter	Value	Unit
Applied voltage	0.5	V/cm
Sediment		
Volume	45	m^3
Resistivity	0.75	Ω m
Electric wire		
Input length	15	m
Radius	1	cm
Resistivity	0.018	Ω m
Graphite electrode		
Height	3	m
Radius	10	cm
Resistivity	7.2	Ω m
Power for instrument management		
pH monitor	0.05	kW
Peristaltic pump	2 × 0.2	
Energy cost	0.09	$/kWh

efficiency, here we defined it as the energy required to decontaminate 1 mg Pb in sediments. Obviously, it experienced an exponential decrease with elapsed time due to the continuous depletion of Pb^{2+} (Fig. 10a). In addition, the energy utilization efficiencies were extremely low during the EPI periods. In this case, a short remediation duration was proposed in order to improve the performance of EPI-EKR.

Same conclusion was achieved when considering the results of cost assessment (Fig. 10b). The cost was strongly dependent on EC and also experienced an exponential growth with continuous remediation. More cost would be required to remove the same amount of Pb as time passed by. Therefore, it is unnecessary to clean up the Pb if its concentration in sediments reached the safety threshold as requested. According to the Control Standards of Pollutants in Sludge for Agricultural Use (GB 4284-2018), the maximum content of Pb is regulated not to exceed 300 mg/kg. Except for this upper limit, a concentration of 220 mg/kg could be regarded as the lower limit in this case since sharp increase of the cost was observed for further decontamination. In that way, a cost varied from 60 to 110 $/m^3$ was assumed for the optimal EPI-EKR to decrease the sediment Pb to the safety range. It should be noted that the present cost analysis was independently assessed based on the simulated EC results. For estimating the performance of pilot EKR project, other costs included the expenditure for materials (e.g., DC power supplier, multimeter, electrodes, electric wires, pipes, etc.), recycling of Pb in electrolyte and labor. In our study, this cost was estimated to be 450 $/remediation unit, 2 $/L and 300 $/remediation unit, respectively. Since the materials could be reused and the labor for manufacturing the EKR plant could be neglected in the following treatments, the total cost for implementing such remediation should be acceptable.

Ecology risk evaluation

Ensuring the ecology safety is an important task for the recycling of metal-polluted sediments for agricultural activities. In the present study, the recycling of sediments with total Pb content of 345.6 mg/kg (EXP 5), 300 mg/kg (EXP 6), and 220 mg/kg (EXP 7) was respectively implemented for vegetable plantation. The results of detected Pb concentrations are shown in Table 3. Obviously, more Pb was found in the soils and vegetables of EXP 5 due to the largest addition of exogenous Pb. In addition, as hyperaccumulator, more Pb was accumulated in *Brassica juncea* than in *Brassica pekinensis* and *Spinacia oleracea L.*

In order to comprehensively estimate the quality of both soils and vegetables influenced by the Pb-polluted sediments, an innovative approach derived from the plant ion impulse and soil relative impact equivalent evaluation method was applied. Initially, the measured Pb in soil samples (C_i) and agricultural products (C_{APi}) were compared with the Pb standard values for soil quality assessment (C_{si}), Pb background value in soil (C_{Bi}), and Pb limit values for food safety (C_{LSi}), respectively. The comparisons were simply expressed as

$$P_{ssi} = C_i/C_{si}; \quad P_{SBi} = C_i/C_{Bi}; \quad P_{APi} = C_{APi}/C_{LSi}, \tag{15}$$

where C_{Bi} was premeasured from the sampling site. C_{si} and C_{LSi} was, respectively, determined as 90 mg/kg and 0.1 mg/kg (Table 3) according to the Soil Environmental Quality Risk Control Standard for Soil Contamination of Agricultural Land (GB15618-2018) and the National Food Safety Control Standard for Contaminant (GB2762-2017). From the obtained data (Table 3), the contents of soil Pb in different experiments were detected between the C_{Bi} and C_{si} which indicated the reasonable quality of soil analyses. However, significant high Pb concentration was discovered in vegetables, especially in *Brassica juncea*, as the increasing of Pb amount in recycling sediments. Thus, we further defined the values of X, Y, and Z to describe the Pb content. If the specific values of P_{ssi}, P_{SBi}, and P_{APi} were larger than 1, the values of X, Y, and Z would be correspondingly set to 1. Conversely, the values of X, Y, and Z would be set to 0.

Subsequently, based on the above comparisons, we could calculate the parameters of relative impact equivalent (*RIE*), deviation degree of determination

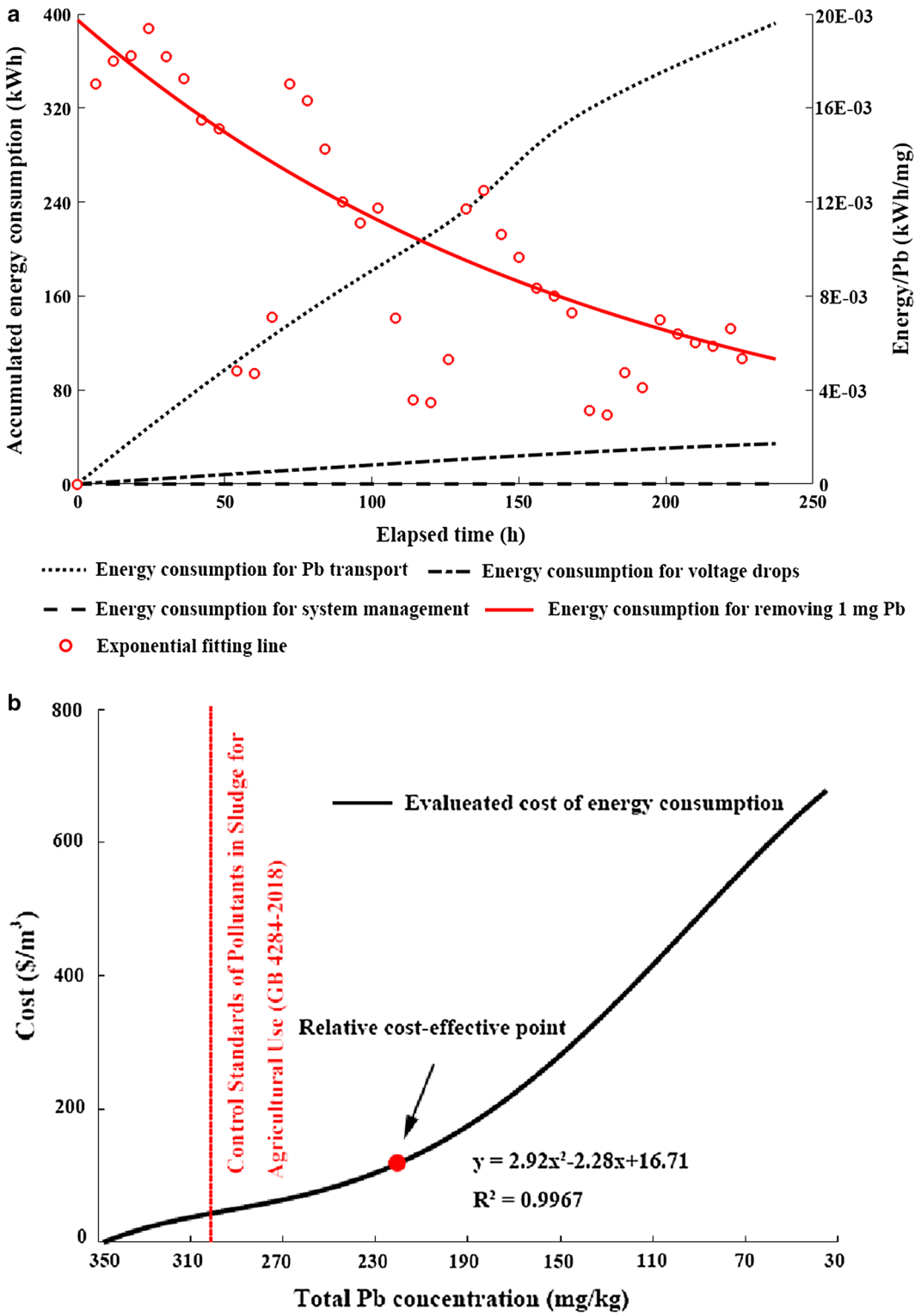

Fig. 10 Energy consumption (**a**) and cost analysis (**b**) of the treated unit area under the optimal EPI-EKR (0.5 V/cm, 12 h of EPI duration). The relative cost-effective point referred to the moment that sharp increase of the energy cost was required to remove 1 mg Pb in sediments

Table 3 Detected Pb concentrations in soils and vegetables after recycling of sediments with Pb content of 346 mg/kg, 300 mg/kg, and 220 mg/kg

EXP	Sample	Pb (mg/kg)			
		Soil	*Brassica juncea*	*Brassica pekinensis*	*Spinacia oleracea L.*
Exogenous Pb (346 mg/kg)	1	46.7	0.32	0.16	0.13
	2	44.1	0.37	0.20	0.16
	3	46.5	0.34	0.15	0.14
	4	45.8	0.43	0.22	0.11
Control standard value[a]		90.0	0.10	0.10	0.10
Background value[b]		18.4	–	–	–
Exogenous Pb (300 mg/kg)	5	39.2	0.27	0.13	0.06
	6	40.9	0.22	0.14	0.09
	7	38.4	0.15	0.09	0.08
	8	39.6	0.18	0.16	0.07
Control standard value		90.0	0.10	0.10	0.10
Background value		16.9	–	–	–
Exogenous Pb (220 mg/kg)	9	25.4	0.09	0.04	0.04
	10	24.3	0.08	0.06	0.02
	11	24.7	0.05	0.07	0.03
	12	23.9	0.07	0.08	0.05
Control standard value		90.0	0.10	0.10	0.10
Background value		17.8	–	–	–

[a] Control standard value: the control standard value of Pb content in soils and vegetables requested by the Soil Environmental Quality Risk Control Standard for Soil Contamination of Agricultural Land (GB15618-2018) and the National Food Safety Control Standard for Contaminant (GB2762-2017)

[b] Background value: the detected Pb content in soils and vegetables without recycling of Pb-polluted sediments

concentration from the background value (*DDDB*), and deviation degree of soil standard from the background value (*DDSB*), respectively, with the following expressions:

$$RIE = \left[\sum_{i=1}^{N} (P_{ssi})^{1/n}\right]/N = \left[\sum_{i=1}^{N} (C_i/C_{si})^{1/n}\right]/N \tag{16}$$

$$DDDB = \left[\sum_{i=1}^{N} (P_{SBi})^{1/n}\right]/N = \left[\sum_{i=1}^{N} (C_i/C_{Bi})^{1/n}\right]/N \tag{17}$$

$$DDSB = \left[\sum_{i=1}^{N} (C_{Si}/C_{Bi})^{1/n}\right], \tag{18}$$

where N was the quantity of the target element and n was the relevant valence of its oxide in soils. Since we only concerned Pb in this case, the values of N and n were accordingly set to 1 and 2. The *RIE* and *DDDB* were the indexes that reflected the impact of exogenous Pb on soil quality while *DDSB* represented the buffering capacity of soil for such pollution. In addition, the quality index of agricultural products (*QIAP*) was estimated as follows:

$$QIAP = \left[\sum_{i=1}^{N} (P_{APi})^{1/n}\right]/N = \left[\sum_{i=1}^{N} (C_{APi}/C_{LSi})^{1/n}\right]/N. \tag{19}$$

This index indicated the fact that, under a pollution situation, the higher of Pb concentration was detected in agricultural products, the poorer of product qualities would be.

Afterwards, the influence indexes of comprehensive quality for soils ($IICQ_S$) and agricultural products ($IICQ_{AP}$) were calculated by

$$IICQ_S = X \bullet (1 + RIE) + Y \bullet DDDB/DDSB \tag{20}$$

$$IICQ_{AP} = Z \bullet (1 + QIAP/k) + QIAP/(k \bullet DDSB), \tag{21}$$

where k is the background correction factor and was set to 5. Finally, the influence indexes of comprehensive quality for agro-ecosystem (*IICQ*) were obtained by summing the value of $IICQ_S$ and $IICQ_{AP}$:

$$IICQ = IICQ_S + IICQ_{AP}. \tag{22}$$

Table 4 showed the calculated indexes for the reference cases. The average value of *IICQ* was clearly increased as the increasing addition of exogenous Pb. Moreover, it

was observed to be larger in *Brassica juncea* plantation than those in *Brassica pekinensis* and *Spinacia oleracea L.* plantation. This was due to the high ability of *Brassica juncea* on Pb accumulation. The *IICQ* value directly reflected the level of ecological risk which was evaluated with the classification criterions according to the Technical Specification for Soil Environmental Quality Assessment (Table 5). Generally, the agro-ecosystem influenced by the untreated Pb-contaminated sediments (EXP 5) was light polluted with *IICQ* ranged from 2.06 to 2.28. This

Table 4 Indexes calculations for ecology risk evaluation after recycling of sediments with Pb content of 346 mg/kg, 300 mg/kg, and 220 mg/kg

EXP	Sample	Soil						*Brassica juncea*			
		RIE[a]	*DDDB*[b]	*DDSB*[c]	$IICQ_S$[d]	*X*[h]	*Y*[h]	*QIAP*[e]	$IICQ_{AP}$[f]	*Z*[h]	*IICQ*[g]
Exogenous Pb (346 mg/kg)	1	0.720	1.620	2.212	0.73	0	1	1.79	1.52	1	2.25
	2	0.701	1.574		0.71	0	1	1.92	1.56	1	2.27
	3	0.719	1.616		0.73	0	1	1.84	1.54	1	2.27
	4	0.713	1.604		0.73	0	1	2.07	1.60	1	2.33
IICQ 1–4 (Average value ± standard deviation):								2.28 ± 0.03			
Exogenous Pb (300 mg/kg)	5	0.660	1.484	2.308	0.64	0	1	1.64	1.47	1	2.11
	6	0.674	1.515		0.66	0	1	1.48	1.43	1	2.08
	7	0.653	1.469		0.64	0	1	1.23	1.35	1	1.99
	8	0.663	1.492		0.65	0	1	1.34	1.39	1	2.03
IICQ 5–8 (Average value ± standard deviation):								2.05 ± 0.06			
Exogenous Pb (220 mg/kg)	9	0.531	1.195	2.249	0.53	0	1	0.95	0.084	0	0.62
	10	0.520	1.168		0.52	0	1	0.89	0.080	0	0.60
	11	0.524	1.178		0.52	0	1	0.71	0.063	0	0.59
	12	0.515	1.159		0.52	0	1	0.84	0.074	0	0.59
IICQ 9–12 (Average value ± standard deviation):								0.60 ± 0.01			

EXP	Sample	*Brassica pekinensis*				*Spinacia oleracea L.*			
		QIAP	$IICQ_{AP}$	*Z*	*IICQ*	*QIAP*	$IICQ_{AP}$	*Z*	*IICQ*
Exogenous Pb (346 mg/kg)	1	1.27	1.37	1	2.10	1.14	1.33	1	2.06
	2	1.41	1.41	1	2.12	1.27	1.37	1	2.08
	3	1.23	1.36	1	2.09	1.18	1.34	1	2.08
	4	1.48	1.43	1	2.16	1.05	1.31	1	2.03
IICQ 1–4 (average value ± standard deviation):		2.12 ± 0.03				2.06 ± 0.02			
Exogenous Pb (300 mg/kg)	5	1.14	1.33	1	1.97	0.78	0.067	0	0.71
	6	1.18	1.34	1	2.00	0.95	0.082	0	0.74
	7	0.95	0.082	0	0.72	1.10	0.075	0	0.73
	8	1.27	1.36	1	2.01	0.84	0.073	0	0.72
IICQ 5–8 (average value ± standard deviation):		1.67 ± 0.64				0.73 ± 0.01			
Exogenous Pb (220 mg/kg)	9	0.63	0.056	0	0.59	0.63	0.056	0	0.59
	10	0.78	0.069	0	0.59	0.45	0.040	0	0.56
	11	0.84	0.074	0	0.60	0.55	0.049	0	0.57
	12	0.89	0.080	0	0.60	0.71	0.063	0	0.58
IICQ 9–12 (average value ± standard deviation):		0.59 ± 0.01				0.57 ± 0.01			

[a] Relative impact equivalent (*RIE*)

[b] Deviation degree of determination concentration from the background value (*DDDB*)

[c] Deviation degree of soil standard from the background value (*DDSB*)

[d] Influence index of comprehensive quality for soil ($IICQ_S$)

[e] Quality index of agricultural product (*QIAP*)

[f] Influence index of comprehensive quality for agricultural product ($IICQ_{AP}$)

[g] Influence index of comprehensive quality for agro-ecosystem (*IICQ*)

[h] Defined values for describing the Pb contents in soils and vegetables (*X*, *Y*, *Z*)

pollution was alleviated in EXP 6 where the Pb content in sediments was decreased to 300 mg/kg as requested by the safety control standard (GB 4284-2018). However, the ecological risks still existed in the plantation of *Brassica juncea* and *Brassica pekinensis* as the obtained *IICQ* was 2.05 and 1.67, respectively. The agricultural environment seemed safe in EXP 7, where the values of calculated *IICQ* were far below 1. This result verified that 220 mg/kg might be the preferable safety threshold for cost-effective decontamination and eco-friendly recycling of Pb-polluted sediments in the present study.

Conclusions

In this paper, an innovative methodology which included modeling and feasibility analysis was proposed for pilot-scale EPI-EKR to remediate and recycle the Pb-polluted field sediments.

Referring to the modeling of EPI-EKR, the operating parameters of the model were initially assumed containing migrating species, diffusion coefficients, sediment physico-chemical characteristics, etc. They were beneficial for accurately reproducing the field geometry as well as reducing the errors during the modeling. The model consisted of two coupled modules that described the transport processes and chemical equilibriums. A set of equations were assumed to predict the electromigration/electroosmosis mechanisms and the precipitation/dissolution and adsorption/desorption behaviors of the sediment Pb.

Afterwards, numerical computation was implemented to simulate the time-dependent pHs and Pb distributions during the treatment. Under constant electric field, stable anionic Pb complexes and precipitations were accumulated around the cathode regions from 48 h. This phenomenon was due to the significant sediment alkalization at that time which formed a dead zone to hinder the transport of Pb^{2+}. Thus, 48 h was suggested to be the proper timing of EPI. Subsequently, the optimization of EPI duration was carried out in consideration of EKR efficiency. Based on the current results, 12 h seemed to be the preferable EPI period since sediment basification was approximately eliminated and no backflow of aqueous Pb was observed. Furthermore, the required time for the optimal EPI-EKR to wipe off 90% of the total Pb was 226 h, which was significantly shorter compared to other tests.

A comparative study was further performed between the predicted and field-scale experimental results in order to validate the accuracy of the model. Overall, good agreements were achieved in spite of minor discrepancies caused by electric field distribution, voltage drops, ions depletion, and sediment Pb speciation. Neglecting of such effects was conformed to have impacts on model simulation as a 5–10% overestimation on Pb removals, while maintained in an acceptable range. Therefore, the designed 2D model could approximately predict the real transport-reactive processes in pilot-scale EPI-EKR.

In terms of feasibility analysis, a parametric study of EC was performed to discriminate between energy losses and energy used effectively for the optimal EPI-EKR. The total EC had an increasing trend with time and the energy expenditure caused by voltage drops and EKR system management only accounted for around 7–9%. It was unnecessary to eliminate the sediment Pb since the energy utilization efficiency was significantly lower in the later stage of the remediation. This conclusion was in accordance with the cost assessment that more expenditure was required to remove the same amount of Pb as time passed by. Thus, the concentration of 220 mg/kg was determined as the lower limit of safety threshold for economy concern. In that way, the maximum EC cost for the treatment of Pb-polluted sediments with EPI-EKR was 110 $\$/m^3$ and other costs for materials expenditure, electrolyte Pb recycling, and labor were estimated to be around 750 \$/remediation unit. Since the materials could be reused and the labor for manufacturing the EKR plant could be ignored, the total cost for the further remediation should be acceptable.

Finally, an innovative approach was applied to estimate the ecological risk induced by the recycling of Pb-polluted sediments. In this part, the *IICQ* which described the quality of both soils and vegetables was calculated. The values of *IICQ* directly corresponded to the ecological risk level and were further classified by the relevant criterions. Light pollution was discovered in agro-ecosystem influenced by the untreated sediments. Such pollution was alleviated when decreased the sediment Pb content to the requested control standard (300 mg/kg). However, pollution situation of Pb still existed in vegetables, especially in hyperaccumulator of *Brassica juncea*. The agricultural environment was safe when using the sediments with Pb concentration of 220 kg/mg for field plantation. This result indicated that 220 mg/kg could be

Table 5 Classification criterions of agricultural environment quality

Value of the *IICQ*[a]	Environment quality state
$IICQ \leq 1$	Clean (I)
$1 < IICQ \leq 2$	Light polluted (II)
$2 < IICQ \leq 3$	Light polluted (III)
$3 < IICQ \leq 5$	Moderate polluted (IV)
> 5	Severe polluted (V)

[a] Influence index of comprehensive quality for agro-ecosystem (*IICQ*): the index for assessing the quality of both soils and agricultural products

the preferable safety threshold for cost-effective decontamination and eco-friendly recycling of Pb-polluted sediments.

In summary, the results in the present study were important in the context of the existing literature and for the practical application of EPI-EKR as a decontamination technology. Moreover, we also believed that the modeling, experimental, and evaluating methodology developed may be applied as an useful tool for the remediation and recycling of metal-polluted sediments.

Abbreviations

EKR: electro-kinetic remediation; EPI: electrode polarity inversion; EPI-EKR: electrode polarity inversion enhanced electro-kinetic remediation; 2D: two dimensional; EC: energy consumption; CEC: cation exchange capacity; OM: organic matter; DOM: dissolved organic matter; ICP-MS: inductively coupled plasma mass spectrometry; EXP: experiment; RIE: relative impact equivalent; DDDB: deviation degree of determination concentration from the background value; DDSB: deviation degree of soil standard from the background value; QIAP: quality index of agricultural products; $IICQ_S$: influence index of comprehensive quality for soil; $IICQ_{AP}$: influence index of comprehensive quality for agricultural product; IICQ: influence index of comprehensive quality for agro-ecosystem; EXT: acid extractable fraction; OXID: oxidizable fraction; RED: reducible fraction; RES: residual fraction.

Author contributions

XM: designation of the model and pilot-scale experiments, implementation of the experiments, data analyzing and processing, and manuscript writing; XS: designation of the model; and ZZ: designation of the pilot-scale experiments. All authors read and approved the final manuscript.

Author details

[1] College of Agricultural Engineering, Hohai University, Nanjing 210098, China. [2] Key Laboratory of Efficient Irrigation-Drainage and Agricultural Soil–Water Environment in Southern China, Ministry of Education, Nanjing 210098, China.

Acknowledgements

The authors would like to thank Hohai University and Key Laboratory of Efficient Irrigation-Drainage and Agricultural Soil–Water Environment in Southern China for the support and assistance provided.

Competing interests

The authors declare that they have no competing interests.

Availability of data and materials

The datasets used and analyzed during the current study are available from the corresponding author on reasonable request.

Consent for publication

Not applicable.

Ethics approval and consent to participate

Not applicable.

Funding

This work was supported by the "National Natural Science Foundation of China"(51809076), the "Fundamental Research Funds for the Central Universities" (2017B11014), and the "China Postdoctoral Science Foundation" (2017M611677).

Publisher's Note

Received: 7 January 2019 Accepted: 25 April 2019
Published online: 03 May 2019

References

1. Han LF, Gao B, Hao H, Zhou HD, Lu J, Sun K (2018) Lead contamination in sediments in the past 20 years: a challenge for China. Sci Total Environ 640–641:746–756
2. Xu D, Wang R, Wang WG, Ge Q, Zhang WL, Chen L, Chu FY (2019) Tracing the source of Pb using stable Pb isotope ratios in sediments of eastern Beibu Gulf, South China Sea. Mar Pollut Bull 141:127–136
3. Wang LQ, Dai LJ, Li LF, Liang T (2018) Multivariable cokriging prediction and source analysis of potentially toxic elements (Cr, Cu, Cd, Pb, and Zn) in surface sediments from Dongting Lake, China. Ecol Indic 94:312–319
4. Pratte S, Bao KS, Shen J, De Vleeschouwer F, Le Roux G (2019) Centennial records of cadmium and lead in NE China lake sediments. Sci Total Environ 657:548–557
5. Kirkelund GM, Ottosen LM, Villumsen A (2010) Investigations of Cu, Pb and Zn partitioning by sequential extraction in harbour sediments after electrodialytic remediation. Chemosphere 79(10):997–1002
6. Yang G, Zhang GM, Wang HC (2015) Current state of sludge production, management, treatment and disposal in China. Water Res 78:60–73
7. Akcil A, Erust C, Ozdemiroglu S, Fonti V, Beolchini F (2015) A review of approaches and techniques used in aquatic contaminated sediments: metal removal and stabilization by chemical and biotechnological processes. J Clean Prod 86(1):24–36
8. Vermeulen J, van Dijk SG, Grotenhuis JTC, Rulkens WH (2005) Quantification of physical properties of dredged sediments during physical ripening. Geoderma 129(3–4):147–166
9. Kim GN, Kim SS, Park UR, Moon JK (2015) Decontamination of soil contaminated with cesium using electrokinetic-electrodialytic method. Electrochim Acta 181:233–237
10. Li TT, Wang Y, Guo SH, Li XY, Xu YN, Wang Y (2016) Effect of polarity-reversal on electrokinetic enhanced bioremediation of Pyrene contaminated soil. Electrochim Acta 187:567–575
11. Kim BK, Baek K, Ko SH, Yang JW (2011) Research and field experiences on electrokinetic remediation in South Korea. Sep Purif Technol 79(2):116–123
12. Yuan LZ, Xu XJ, Li HY, Wang NN, Guo N, Yu HW (2016) Development of novel assisting agents for the electrokinetic remediation of heavy metal-contaminated kaolin. Electrochim Acta 218:140–148
13. Kim WS, Park GY, Kim DH, Jung HB, Ko SH, Baek K (2012) In situ field scale electrokinetic remediation of multi-metals contaminated paddy soil: influence of electrode configuration. Electrochim Acta 86(1):89–95
14. Alcántara MT, Gómez J, Pazos M, Sanromán MA (2012) Electrokinetic remediation of lead and phenanthrene polluted soils. Geoderma 173–174:128–133
15. Mao XY, Han FX, Shao XH, Arslan Z, McComb J, Chang TT, Guo K, Celik A (2016) Remediation of lead-, arsenic-, and cesium-contaminated soil using consecutive washing enhanced with electro-kinetic field. J Soil Sediment 16(10):2344–2353
16. Mao XY, Han FX, Shao XH, Guo K, McComb J, Njemanze S, Arslan Z, Zhang ZY (2016) The distribution and elevated solubility of lead, arsenic and cesium in contaminated paddy soil enhanced with the electrokinetic field. Int J Environ Sci Technol 13(7):1641–1652
17. Ait Ahmed O, Derriche Z, Kameche M, Bahmani A, Souli H, Dubujet P, Fleureau JM (2016) Electro-remediation of lead contaminated kaolinite: an electro-kinetic treatment. Chem Eng Process 100:37–48
18. Alshawabkeh AN (2009) Electrokinetic soil remediation: challenges and opportunities. Sep Sci Technol 44:2171–2187
19. Mao XY, Shao XY, Zhang ZY, Han FX (2018) Mechanism and optimization of enhanced electro-kinetic remediation on ^{137}Cs contaminated kaolin soils: a semi-pilot study based on experimental and modeling methodology. Electrochim Acta 284:38–51
20. Jacobs RA, Probstein RF (1996) Two-dimensional modeling of electroremediation. AIChE J 42:1685–1696

21. Vereda-Alonso C, Miguel Rodríguez-Maroto J, García-Delgado RA, Gómez-Lahoz C, García-Herruzo F (2004) Two-dimensional model for soil electrokinetic remediation of heavy metals: application to a copper spiked kaolin. Chemosphere 54:895–903
22. Johannesson B (2010) Development of a generalized version of the Poisson–Nernst–Planck equations using the hybrid mixture theory: presentation of 2D numerical examples. Transp Porous Media 85:565–592
23. Al-Hamdan A, Reddy K (2008) Electrokinetic remediation modeling incorporating geochemical effects. J Geotech Geoenviron Eng 134:91–105
24. Paz-García JM, Johannesson B, Ottosen LM, Ribeiro AB, Rodríguez-Maroto JM (2011) Modeling of electrokinetic processes by finite element integration of the Nernst-Planck-Poisson system of equations. Sep Purif Technol 79:183–192
25. Rubio-Nieblas V, Perez-Tello M, Jacobs RA, Herrera-Urbina R (2014) Two dimensional computational modeling of the electrokinetic remediation of a copper-contaminated soil part II: sensitivity analysis for a triangular soil field. Dyna 81(183):199–207
26. Masi M, Ceccarini A, Iannelli R (2017) Multispecies reactive transport modelling of electrokinetic remediation of harbour sediments. J Hazard Mater 326:187–196
27. Gomes HI, Rodríguez-Maroto JM, Ribeiro AB, Pamukcu S, Dias-Ferreira C (2015) Numerical prediction of diffusion and electric field-induced iron nanoparticle transport. Electrochim Acta 181:5–12
28. Paz-García JM, Villén-Guzmán M, García-Rubio A, Hall S, Ristinmaa M, Gómez-Lahoz C (2016) A coupled reactive-transport model for electrokinetic remediation. In: Ribeiro AB, Mateus EP, Couto N (eds) Electrokinetics across disciplines and continents. Springer International Publishing, Switzerland
29. Zoller WH, Gladney ES, Duce RA (1974) Atmospheric concentrations and sources of trace metals at the South Pole. Science 183(4121):198–200
30. Müller G (1979) Schwermetalle in den sedimenten des rheinsver nderungen seit 1971. Umschau in Wissenschaft und Technik 79(24):778–783
31. Håkanson L (1980) The quantitative impact of pH, bioproduction and Hg -contamination on the Hg-content of fish (pike). Environ Pollut Ser B Chem Phys 1(4):285–304
32. Cheng JL, Zhou S, Zhu YW (2007) Assessment and mapping of environmental quality in agricultural soils of Zhejiang Province, China. J Environ Sci 19(1):50–54
33. Parkhurst DL, Wissmeier L (2015) PhreeqcRM: a reaction module for transport simulators based on the geochemical model PHREEQC. Adv Water Resour 83:176–189
34. Masi M, Ceccarini A, Iannelli R (2017) Model-based optimization of field-scale electrokinetic treatment of dredged sediments. Chem Eng J 328:87–97
35. Shackelford C, Daniel D (1991) Diffusion in saturated soil. I: background. J Geotech Eng 117:467–484
36. Fan G, Long C, Fang G, Zhou D (2014) Surfactant and oxidant enhanced electrokinetic remediation of a PCBs polluted soil. Sep Purif Technol 123:106–113
37. Qiu LW, Shen YD, Wang C (2017) pH- and KCl- induced formation of worm-like micelle viscoelastic fluids based on a simple tertiary amine surfactant. J Pet Sci Eng 162:158–165
38. Mao XY, Han FX, Shao XH, Guo K, McComb J, Arslan Z, Zhang ZY (2016) Electro-kinetic remediation coupled with phytoremediation to remove lead, arsenic and cesium from contaminated paddy soil. Ecotox Environ Safe 125:16–24
39. Pazos M, Sanromán MA, Cameselle C (2006) Improvement in electrokinetic remediation of heavy metal spiked kaolin with the polarity exchange technique. Chemosphere 62:817–822
40. Kim KJ, Kim DH, Yoo JC, Baek K (2011) Electrokinetic extraction of heavy metals from dredged marine sediment. Sep Purif Technol 7(2):164–169
41. Jansen B, Nierop KGJ, Verstraten JM (2002) Influence of pH and metal/carbon ratios on soluble organic complexation of Fe(II), Fe(III) and Al(III) in soil solutions determined by diffusive gradients in thin films. Anal Chim Acta 454:259–270
42. Wang WH, Chen M, Guo LD, Wang WX (2017) Size partitioning and mixing behavior of trace metals and dissolved organic matter in a South China estuary. Sci Total Environ 603–604:434–444
43. Villen-Guzman M, Paz-Garcia JM, Amaya-Santos G, Rodriguez-Maroto JM, Vereda-Alonso C, Gomez-Lahoz C (2015) Effects of the buffering capacity of the soil on the mobilization of heavy metals: equilibrium and kinetics. Chemosphere 131:78–84